

**Role of protein aggregate structure on the strength and underwater performance of barnacle-inspired adhesives**

Journal:	<i>Soft Matter</i>
Manuscript ID	SM-ART-03-2023-000342.R1
Article Type:	Paper
Date Submitted by the Author:	01-May-2023
Complete List of Authors:	Wilson, Michael; US Naval Research Laboratory, NRC Postdoctoral Associate sited in Chemistry Division, Code 6176 Beasley, Maryssa; US Naval Research Laboratory, NRC Postdoctoral Associate sited in Chemistry Division, Code 6176 Fears, Kenan; Naval Research Laboratory Chemistry Division Yates, Elizabeth; US Naval Research Laboratory, U.S. Naval Academy faculty sited in Chemistry Division, Code 6176 So, Christopher; Naval Research Laboratory Chemistry Division, Chemistry

Role of protein aggregate structure on the strength and underwater performance of barnacle-inspired adhesives

Michael C. Wilson¹, Maryssa A. Beasley¹, Kenan P. Fears², Elizabeth A. Yates³, Christopher R.

So^{2}*

¹NRC Postdoctoral Associate sited in Chemistry Division, Code 6176, U.S. Naval Research
Laboratory, Washington, DC

²Chemistry Division, Code 6176, U.S. Naval Research Laboratory, Washington, DC

³U.S. Naval Academy faculty sited in Chemistry Division, Code 6176, U.S. Naval Research
Laboratory, Washington, DC

Corresponding Author

*christopher.so@nrl.navy.mil

ABSTRACT

Nature employs protein aggregates when strong materials are needed to adhere surfaces in extreme environments, allowing organisms to survive conditions ranging from harsh intertidal coasts to open oceans. Amyloids and amyloid-like materials are prevalent and amongst the most densely bonded aggregate structures, though how they contribute to wet adhesion is not well understood.

In this work, waterborne protein solutions of individual whey proteins are cured in place using varied temperature to produce model adhesives enriched in amyloid or non-amyloid aggregates.

Dry adhesive strengths range from 0.2 – 1.5 MPa, while wet adhesive strengths range from 0 – 0.5 MPa across the tested proteins and processing conditions, highlighting that both proper protein selection and controlled aggregation extent are necessary for successful underwater performance.

For bovine serum albumin, the amyloid-enriched adhesive was able to retain ca. 500 kPa bond

strength underwater throughout extended immersion and thermal degradation testing, while the non-amyloid adhesive weakened by up to 80%. As freestanding gels, higher temperature processing improved underwater stability for all protein materials, with amyloid-rich structures remaining mostly water-insoluble after 30 days submerged in water. Protein-based adhesives with controlled aggregate structure shed light on the ability of amyloid-containing materials to remain adhered underwater, a necessary trait for the survival of many organisms.

INTRODUCTION

Protein structure dictates properties not only at the molecular level, but also the mechanical properties of bulk materials when used over large scales. To achieve intricate hierarchy and function, organisms use complex biological systems to control the structure and aggregation state of proteins. Adhesion—specifically adhesives that work underwater—is one area where this is abundantly observed. Protein aggregation plays a key role in the success of bacterial biofilms,¹ mussel byssus,^{2,3} barnacle cement,⁴⁻⁶ caddisfly silk,⁷ and algal glue,⁸ creating robust materials with structural integrity in harsh, abiotic environments.

Hierarchical assembly of aggregates and their formation into bulk materials often occurs outside of the organism, at the site where they are needed. In particular, many organisms use organized aggregates known as amyloids to build structures in wet environments.^{1, 8-12} One particularly masterful user is the common marine barnacle (Figure 1a), belonging to a cosmopolitan group of crustaceans which form an adhesive plaque containing amyloid-like materials that provides permanent adhesion underwater.^{5, 9} Other amyloid systems, similar to that of the barnacle, have demonstrated properties useful for underwater adhesion: they can be triggered in place,^{13, 14} exhibit high stiffness,¹⁵ provide toughness,^{8, 16} and are highly insoluble.¹⁷ These properties arise from the unique organization of amyloids that span length scales from a β -strand, to cross β -sheets, and ultimately higher order fibrils.¹⁸

Recently, adhesives based on commonplace proteins have been successfully developed for wet applications, such as medical adhesives. Protein-based adhesives across applications typically use free proteins and succeed through their formulation, chemical crosslinking, chemical modification, or designed sequence.¹⁹⁻²² While such adhesives have been widely studied and applied,²³⁻²⁵ the role of protein aggregation state on wet adhesion—especially for amyloids—still remains largely unknown.²⁶ To better determine the role of aggregation on water resistance for protein adhesives,

a model system requires changing aggregate structure while minimizing changes to chemical composition, testing by a standardized bulk adhesion measurement, and application without the use of chemical crosslinkers.

We propose that thermally cured components of whey protein (β -Lactoglobulin, bovine serum albumin, and α -Lactalbumin) can serve as model adhesives to understand how aggregation state influences underwater performance. They are highly soluble in water, so it is possible to attain solution concentrations that approach those of polymer-based glues. They readily form amyloids and other aggregates under changing environmental conditions without the addition of covalent crosslinkers or multivalent metal ions.^{13, 18, 25} Because it is possible to achieve different aggregate structures from the same protein,^{18, 27, 28} the sequence and chemistry can remain unchanged while varying the structure.

Here, we investigate the role of protein aggregation in underwater performance by independently varying aggregate structure of the individual whey proteins using steam-curing (Figure 1b). Previous procedures typically convert solutions of 2-5% (w/v) protein using with low pH (pH 2),^{29, 30} added salt (NaCl),^{29, 30} added reducing agents (e.g. dithiothreitol),²⁸ and elevated temperature (37-80 °C).²⁸⁻³¹ In our case, we aim to aggregate proteins at much higher concentration without the

use of chemical denaturants, changes to pH, or the addition of salts that could alter the protein chemical functionality in addition to changing the structure. Instead, deposition of the solution and simple change in temperature can trigger the aggregation of the proteins at the interface to form adhesives.¹⁸

To measure the underwater performance of model protein adhesives, we 1) establish conditions which form solid gels and assess their protein structure, morphology, and solubility, 2) trigger targeted aggregation states between lap samples for bond strength measurements, and 3) perform long-term underwater testing and accelerated degradation to determine bond durability of aggregation states. We find that while amyloid-enriched adhesives attain similar bond strengths as their non-amyloid counterparts for the proteins studied, amyloids provide significant underwater durability to the protein materials. Proteins found to have poor intrinsic adhesion, such as β -lactoglobulin, demonstrate that enrichment in the amyloid phase does not lead to enhanced adhesive strength, but still maintain a high insolubility as bulk gels. In the case of bovine serum albumin (BSA), amyloid-enriched adhesives retain nearly 100% of their bond strength after long-term soaking and accelerated thermal degradation, highlighting its ability as a durable adhesive and shedding light on the preference for organisms to use amyloids.

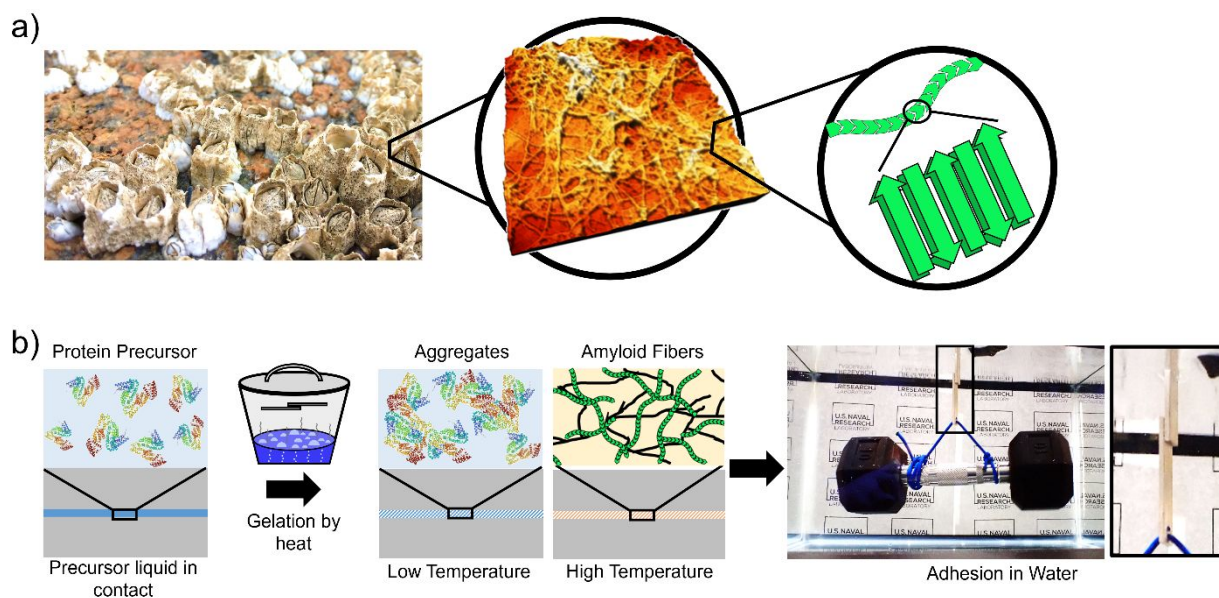


Figure 1. Model amyloid adhesive design. a) Hierarchical structure of barnacle amyloid plaque. b)

Steam curing process employed to form adhesives from non-amyloid aggregates at low temperature and amyloid-based adhesives at high temperature. After this steam process, two aluminum pieces glued together with 0.5 in x 0.5 in adhesive can hold a 10 lb weight underwater, as shown in the black box.

MATERIALS AND METHODS

Protein Solution Preparation. β -Lactoglobulin (β -Lg) ($\geq 90\%$) and bovine serum albumin (BSA) ($\geq 96\%$) were purchased from Millipore-Sigma. BiPRO Alpha 9000, α -Lactalbumin (α -La), was kindly provided by Agropur, Inc. From the manufacturer, 97.8% of the dry material was protein,

with 91.3% of that protein being α -Lactalbumin (α -La). This matches our own gel electrophoresis (Figure S1) which also shows a purity of *ca.* 90% with the main impurity being β -Lg. All proteins were used as is from the manufacturer with no further purification. The proteins were dissolved at room temperature in ultrapure water (Millipore, 18.2 M Ω /cm) by end-over-end rotation at 10-20 rpm.

Gelation Determination and Thioflavin T (ThT) Fluorescence Microscopy. Solution concentration was varied from 50 mg protein / 1 mL water to 500 mg protein / 1 mL water (with all samples labeled as 5% (w/v) to 50% (w/v)). Samples were used within 48 hours of mixing. A stock solution of 5mM Thioflavin T (ThT, Sigma Aldrich) was prepared and added to the protein solutions to achieve a working solution of 500 μ M. A range of solution concentrations were produced for each protein (β -Lg: 25%, 20%, 15%, 10%, 5%; α -La: 50%, 40%, 30%, 20%, 10%, 5%; BSA: 40%, 30%, 20%, 10%, 5%). Samples of 400 μ L were placed in 1.5mL centrifuge tubes and heated in a heating block (Eppendorf Thermomixer C) at temperatures from 50-100 $^{\circ}$ C for 15-180 min without shaking. Gelation was determined using inversion of sample tubes. A binary scale was used to consider gelation; either the solution remained liquid, or it formed a gel.

The samples were also examined using ThT fluorescence microscopy at 480 nm to examine ThT binding to beta-sheet-rich structures.³² The samples were opened, placed in a tube rack, and imaged from the top using a Nikon AZ100 with a 1X Apo objective. The microscope was focused on the top of the tube. An exposure time of 3s was used for all samples, and the light and aperture settings were kept constant across images. Images were cropped but used without further processing.

Gel Electrophoresis Sample Preparation and Testing. Protein gels were formed by heating 20 μL of solution and then were submerged in 1 mL of water for 72 hours to extract soluble components. The water was decanted and 200 μL of Laemmli buffer (2% SDS, 10% glycerol, 5% beta-mercaptoethanol, 0.5% bromophenyl blue) was added to the protein gel. Laemmli buffer was produced from a 2X concentrate (Bio-Rad Laboratories) and beta-mercaptoethanol (ThermoFisher) and stored at $-20\text{ }^{\circ}\text{C}$ until use. The sample and buffer was then heated at $95\text{ }^{\circ}\text{C}$ for one hour and the Laemmli buffer was then decanted. 15 μL of diluted solution from the water extraction and from the Laemmli extraction were added to precast Polyacrylamide gels (Mini-PROTEAN TGX, Bio-Rad Laboratories) in SDS buffer. Gels were run at a fixed voltage of 200 Volts (BioRad PowerPac Basic). They were then stained using protein stain (Imperial Stain,

ThermoFisher Scientific) for one hour and destained using deionized water for at least 24 hours.

The water was changed at least once.

Images of the gels backlit by a ViewOne LabLite (Embi Tec) were taken using a ChemiDoc Imaging System (BioRad Laboratories) with an exposure time of 0.004 s. Band intensity was determined using the Analyze Gel function of ImageJ (National Institutes of Health). Densitometry calibration curves were produced for each protein, and dilution factors were selected to ensure that the final protein concentrations were within the linear regime of the standard curve (Figure S2). Protein concentrations in each extraction were determined via densitometry in comparison to both a standard included on that same gel and to the standard curve for that protein. The entire process of solution curing, extraction, and gel electrophoresis was repeated three times for each sample.

For long term analysis of solubility, the protein gels were submerged in water for 30 days before following the same procedure as the 3-day samples. Statistical comparisons (one tail t-test; mean extracted 3-day \leq mean 30-day extracted) were computed using Igor 8.04.

Additionally, 25% (w/v) β -Lg samples were heated in sealed tubes in the steaming chamber (Instant Pot Ultra Series) to confirm steam heating produced similar materials. (Figure S3)

Transmission Fourier-Transform Infrared Spectroscopy. 20 μL of protein solution (25% (w/v) β -Lg, 40% BSA, or 50% α -La) in D_2O were placed in a transmission cell with heating capabilities (Harrick) between two CaF_2 windows without a spacer. The windows were cleaned with water and methanol before use. Spectra were collected over 64 scans with a resolution of 2 cm^{-1} using a Nicolet 6700 spectrometer (ThermoFisher Scientific) equipped with a deuterated triglycine sulfate (DTGS) detector. A background air spectrum was collected over 64 scans just before examining each sample. Then, a spectrum was collected for the sample at room temperature. A thermal controller (Harrick) was used to heat the cell to $60\text{ }^\circ\text{C}$, $70\text{ }^\circ\text{C}$, or $90\text{ }^\circ\text{C}$ at a rate of $10\text{ }^\circ\text{C}/\text{min}$ without removing it from the instrument. The sample was held at this temperature for 90 min and then passively cooled to room temperature ($\sim 1.5\text{ hr}$). A second spectra was collected at room temperature.

Secondary structure analysis was performed in OriginPro 2021. Second derivatives of the spectra were taken using the Savitsky-Golay function in Origin with a window size of 9. The peaks were then fit using the peak analyzer in Origin. An asymmetric least squares smoothing baseline was added with an asymmetric factor of 1, a threshold of 0.01-0.05, and a smoothing factor of 4. The second derivative spectra were fit using 6-10 peaks, with a FWHM constrained to 15 or 20 if the

fitting forced an unreasonably wide peak. Peak locations were used to assign their secondary structure,³³⁻³⁵ and the peak area was used to estimate fraction. An example fit is provided in the Supplemental Material (Figure S4).

Attenuated Total Reflection Fourier-Transform Infrared Spectroscopy on Steamed Gels. Water (800 mL) at the base of the steaming chamber (Instant Pot Ultra Series) was preheated to the desired temperature shortly before sample preparation. The temperature of the steaming chamber was calibrated by heating 45 mL of water in a 50 mL conical tube (Corning) placed on a wire-rack steamer tray for 90 min and measuring the temperature of the water immediately after.

For sample preparation, 10 μ L of protein solution was placed on a poly(tetrafluoroethylene) block resting on a wire-rack steamer tray in the steaming chamber. A second poly(tetrafluoroethylene) block was placed on the sample. Samples were cured either at 60 °C, 70 °C, or 90 °C and immediately removed from the steaming chamber after 90 min. Samples were dried at least overnight in a desiccator. Control samples were fabricated by casting protein solutions on glass and placing directly into the desiccator.

Fourier-transform infrared spectroscopy was performed in attenuated total reflectance geometry (ATR-FTIR) on a single-bounce diamond prism (Pike Technologies) using a Nicolet 6700 spectrometer (ThermoFisher Scientific). To remove as much water signal as possible, the beamline and the ATR accessory were purged with nitrogen. Spectra were recorded with 4 cm^{-1} resolution using a liquid-nitrogen cooled mercury cadmium telluride (MCT/B) detector. Both background and sample collection were averaged over 2048 scans. The prism was cleaned with ethanol after each sample. Two repeats were taken for each protein from a given processing temperature.

Spectra were analyzed using second derivative analysis. Savitsky-Golay second derivatives were taken with a 9 point window using a second-order polynomial in Omnic software.³³ No other smoothing was applied.

Scanning Electron Microscopy on Steamed Gels. Samples for scanning electron microscopy were prepared in a similar manner to samples for infrared spectroscopy with the following changes. Samples were cast from 900 μL of protein solution in a 2 mm thick O-ring resting on the poly(tetrafluoroethylene) block and then covered with the other block. After immediate removal,

the gels were cut from the O-ring using a circle punch and submerged in liquid nitrogen for at least 1 min, and then lyophilized.

Cross-sectional images were taken by breaking the samples by hand. Samples were then sputter coated with ca. 3 nm of gold to reduce charging. Scanning electron microscopy was performed using a FEI Helios G3 FIB-SEM, with images taken at 25,000X magnification and 5 kV. Post-processing of brightness and contrast were performed in GIMP 2.10.30. Since images were cropped for inclusion as zoomed-in images, full images are provided in the Supplemental Material (Figure S5-S10).

Adhesive Sample Preparation. A lap shear geometry was chosen to test the adhesive strength. Unanodized aluminum flat bar (0.5 in. wide and 0.125 in. thick) was purchased from local hardware stores and cut into samples 2.5 in. long. A 0.25 in. diameter hole was drilled near the end of the sample. To minimize the effect of varying roughness, samples were sanded at 200 rpm first using P1200 and then P4000 grit sandpaper on a Struers Labosystem. Samples were sonicated in deionized water for 30 min and rinsed with ethanol before use.

10 uL of protein solution (25% (w/v) β -Lg, 40% BSA, or 50% α -La) was dispensed onto one adherend of the lap shear sample resting on a homebuilt fixture (Figure S11a). The top adherend was placed with a half-inch overlap, held in place by an aluminum bar, and secured using individual hand-tightened screws (Figure S11b). Lap shear samples were placed in a preheated steaming chamber and cured at 60-90 °C for 90 min. The samples were cooled in the closed steaming chamber overnight before removal to prevent rapid changes in temperature or humidity. Samples were then either placed in a desiccator to dry or submerged in water for 72-96 hr. Adherends were reused after testing. The adhesive residue was removed by hand using coarse sandpaper (either P250, P400, or P600), and adherends were repolished using the aforementioned procedure.

Accelerated water degradation, based on the two-cycle boil test,^{36, 37} was performed on samples prepared using the same procedure as above, with the following additions. After removal from the commercial pressure cooker, samples were placed in water for twelve days. The samples were then placed in a beaker filled with deionized water at around 65 °C on a hot plate without stirring for four hours. Additional water was added as it evaporated to ensure the lap joint remained submerged over the course of heating. Samples were cooled in air and placed back in room temperature water

overnight. The following day, the samples were placed in 65 °C water for another four hours, cooled in air, and then submerged in room temperature water. Samples were then immediately tested for lap shear strength.

Adhesion Testing and Sample Characterization. Lap shear testing was performed on an Instron 68SC-05 (equipped with a 500N load cell) using homebuilt grips consisting of clevis rod ends (Figure S12).³⁸ Samples were pulled at a rate of 1.5 mm/min (estimated as $\sim 0.4 \text{ s}^{-1}$ based on the applied volume of glue and overlap area). Wet adhesion samples were removed from water just before use, without any drying. Any samples that fell apart during curing were not included in the data set, but samples which broke during equilibration were considered to have adhesion strength of 0 MPa. Samples were converted from maximum force (N) to adhesion strength (MPa) using the area of overlap in the lap sample. The samples were then imaged using a Nikon AZ100 microscope with a 0.5X Apo objective. Using ImageJ, the nominal contact area was calculated from the average of three length and width measurements. The sample size is listed in the supplemental material along with average force and average area (Table S1). Samples with areas not measured are noted in the Supplemental Material (Table S1), and the average area from the entire set was

used to estimate their area. When degraded samples are compared to short-term soaking, one-tailed t-tests are performed testing if the adhesion strength of degraded samples are less than the short-term adhesion strength (OriginPro 2021).

Select samples were stained with protein stain (Imperial stain, ThermoFisher Scientific) over multiple cycles with an equivalent time in deionized water until the stain provided visual contrast.

Both adherends of a lap shear sample were stained and destained at the same time.

RESULTS

Thermal curing determines physical state and solubility of protein gel materials.

To establish conditions for curing protein adhesives, we first determine the bulk properties of gels and their underwater performance using protein solutions heated at different temperatures. The gelation behavior, distribution of aggregate states, amyloid formation, and microstructure were examined for protein solutions heated at different temperatures.

First, to relate curing and sample conditions to physical state, solutions of each protein were heated at various concentrations (50-500 mg/mL) across temperatures (50-100 °C) and heating times (15 min, 45 min, 90 min, 180 min). The necessary conditions were identified for gelation by inverting the sample tubes (Figure 2a-b, Figure S13-S15). In general, gelation temperatures reflected the melting point of proteins in the study found between 60-70°C,³⁹⁻⁴³ indicating that

gelation is a result of protein denaturation. The gels rapidly formed above threshold conditions, where higher concentrations and temperatures resulted in stiffer gels. Notably, water is expelled from the hydrogel under certain curing conditions (Figure 2c), indicating that the formed gel contains less water than the initial solution. Additionally, all three proteins facilitate an increase in the fluorescence intensity of ThT at the emission wavelength (480 nm), indicating conversion to beta-sheet-rich structure (Figure 2d).³² In general, heating for 180 min reduced the fluorescence compared to heating for 90 min (Figure S16), so 90 min was chosen as the curing time for further testing.

After establishing physical states of gels, the structure and solubility in water were assessed by monitoring protein loss after exposure to degrees of solubilizing conditions. Protein aggregation processes yield a variety of species that span monomeric, oligomeric, and amyloid states,⁴⁴ which vary in their solubility.^{17, 45, 46} Through this route, it is possible to select processing conditions that produce protein glues with different structures. There are three main protein states based on these solubility properties: the water-soluble diffuse fraction, the Laemmli-soluble fraction consisting of oligomers, and an insoluble fraction with oligomers and amyloids.⁴⁷⁻⁴⁹ Quantification of the pure protein band from gel electrophoresis allows us to determine the fraction of protein removed

and the fraction of remaining insoluble material (Figure 2e-f, Table S2). The protein gels formed more water- and Laemmli-soluble material at lower temperatures and/or lower concentrations than the gels formed at high temperatures and high concentrations. All three proteins cured at high temperature show little dissolution in water. This result further confirms the ability of thermal aggregation to produce insoluble gels.

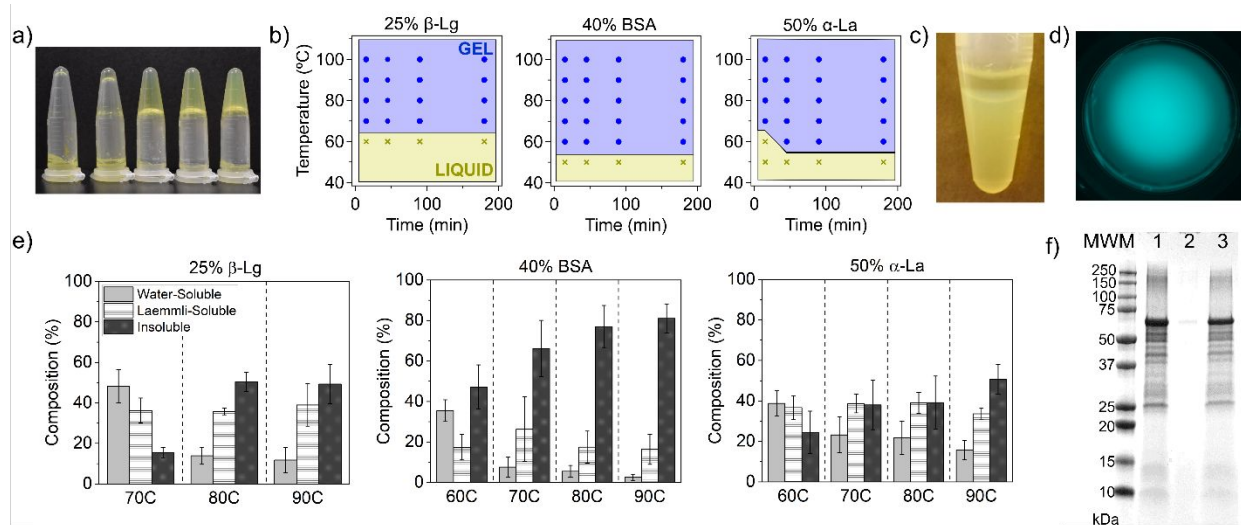


Figure 2: a) Example of solidification of β -Lg solutions at 80 °C for 180 min as a function of concentration. From left: 5%, 10%, 15%, 20%, and 25% (w/v). b) Processing diagram of β -Lg solutions of 25%, BSA solutions of 40% (w/v) and α -La solutions of 50% (w/v) heated at different temperatures and times. Blue circle is gel and yellow x is liquid as determined by inversion. c) Liquid expelled on top of gel during gelation. d) ThT fluorescence of β -Lg at 25%

(w/v), heated at 90 °C for 90 min e) Composition of β -Lg, BSA, and α -La gels cured at different temperatures determined from gel electrophoresis (SDS-PAGE). f) Example SDS-PAGE for 30% BSA. MWM: Molecular weight markers, Lane 1: BSA monomer control, Lane 2: 90 °C curing water-soluble fraction, Lane 3: 90 °C curing Laemmli-soluble fraction; (original image, Figure S17)

Curing conditions produce model materials with amyloid and non-amyloid protein structures and morphologies.

As physical state and solubility provide only a partial window into the aggregation of proteins, we next interrogate the proteins gels by Fourier transform infrared spectroscopy (FTIR) and scanning electron microscopy (SEM). For this, two curing temperatures were selected from each protein. Based on gelation temperature, 60 °C was used for BSA and α -La while 70 °C was used for β -Lg as a low temperature cure. The high temperature cure for all proteins was 90 °C.

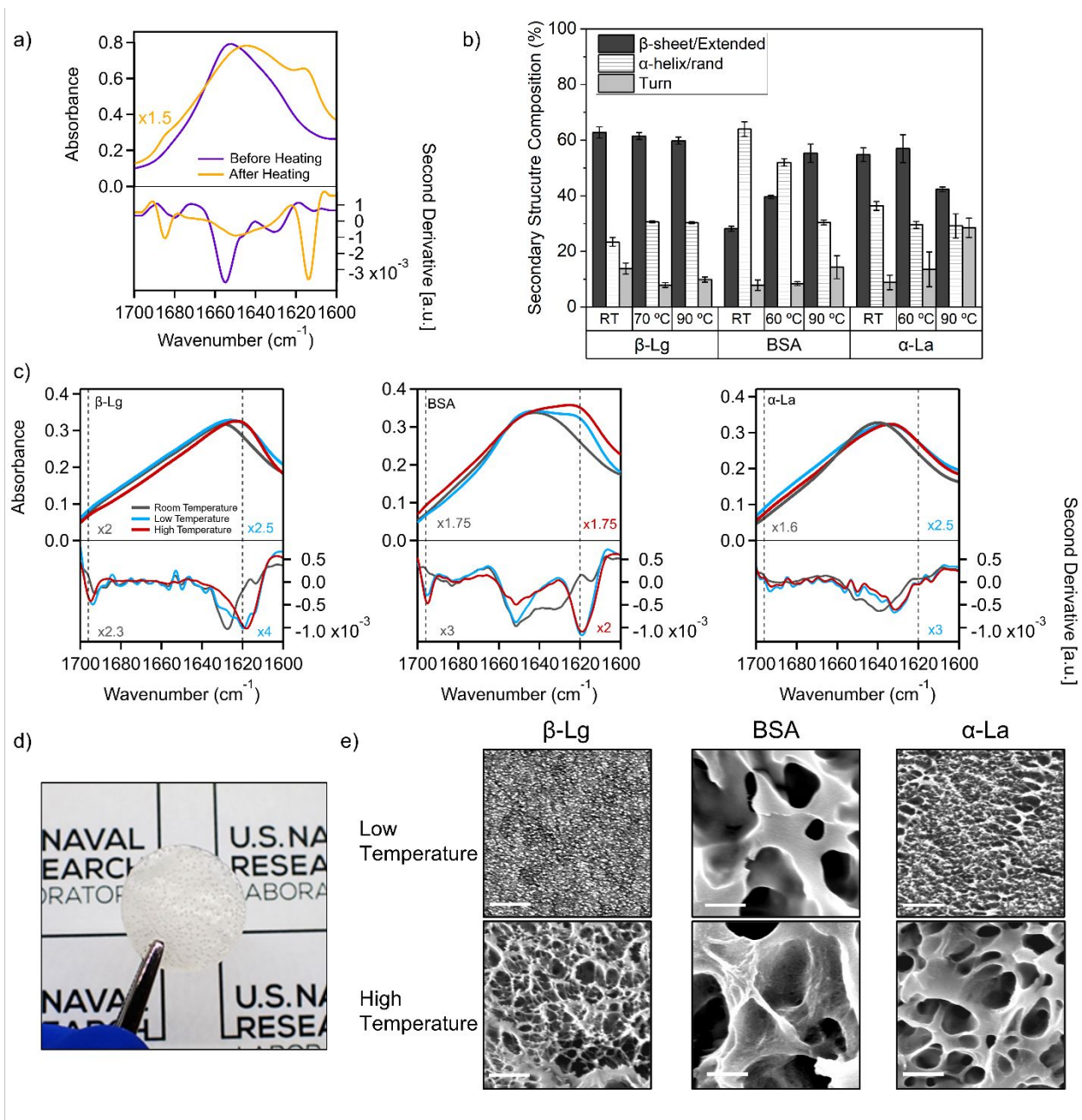


Figure 3. a) Transmission FTIR of BSA in D₂O before and after heating to 90 °C for 90 min and then cooling. b) Composition of secondary structure determined by peak fitting of second derivative transmission FTIR spectra. Error bars represent standard error for n=2. c) ATR-FTIR

of β -Lg, BSA, and α -La cured at different temperatures and then dried. Low temperature curing for β -Lg is 70 °C and for BSA and α -La is 60 °C. High temperature is 90 °C for all proteins. All FTIR spectra are collected at room temperature. Scaling factor is included when used. d) Example protein gel after steam curing. e) SEM of freeze-dried β -Lg, BSA, and α -La after low and high temperature curing. The scale bar indicates 500 nm.

In situ transmission FTIR in D₂O can be used as a method to probe the secondary structure of protein materials exposed to the adhesive processing steps in this work (Figure 3a, Figure S18). For β -Lg, the overall secondary structure does not drastically change after curing at 70 °C or 90 °C (Figure 3b), though the peak positions assigned to β -sheet/extended conformations do change (Table S3). On the other hand, BSA increases in β -sheet/extended conformations from RT to 60 °C to 90 °C, and α -La increases in turns from 60 °C to 90 °C. However, both BSA and β -Lg show peaks below 1620 cm⁻¹ after curing above 60 °C (Table S3), indicative of the cross- β -sheet structure of amyloids.⁵⁰ In contrast, α -La does not show spectral features indicative of this structure.

To confirm the formation of amyloids in samples produced in a steaming chamber, gels cast from the protein solutions were examined after drying using ATR-FTIR. Both heated samples of BSA again show the development of a peak centered at $\sim 1620\text{ cm}^{-1}$, with BSA samples cured at $90\text{ }^{\circ}\text{C}$ showing higher relative intensity (Figure 3c). The secondary structure of dried β -Lg is primarily β -sheet/extended conformation with a peak centered at $\sim 1629\text{ cm}^{-1}$ (Figure 3c). As the curing temperature increases, the peak at 1620 cm^{-1} increases relative to the peak at 1629 cm^{-1} , which is more clearly observed in the second derivative. Overall, the steamed samples match the general trend observed in the transmission FTIR experiments, where β -Lg and BSA form amyloids, and α -La lacks vibration modes indicative of amyloids.

Morphology can serve as a second indicator of differences in structure, with amyloids manifesting as long, discrete, fibrillar structures. All of the systems form gels after steaming (e.g. Figure 3d), which shared an interconnected morphology and a porous network (except at $70\text{ }^{\circ}\text{C}$ curing for β -Lg). However, differences can be seen through SEM in the hierarchical structure defined by aggregate types. BSA cured at $60\text{ }^{\circ}\text{C}$, β -Lg cured at $70\text{ }^{\circ}\text{C}$ and α -La cured at $90\text{ }^{\circ}\text{C}$ do not form clear fibrils (Figure 3e). BSA and β -Lg cured at $90\text{ }^{\circ}\text{C}$ form a network of fibrils. α -La cured at $60\text{ }^{\circ}\text{C}$ forms a mixture of spherical aggregates and fibrillar strands.

Underwater stability testing and adhesion highlight role of aggregate structure on material performance

To understand underwater stability of protein gels over longer periods, we again use gel electrophoresis to quantify the change in aggregate composition of materials upon longer periods of soaking (Table 1). Overall, with both short- and long-term treatments in water, higher temperatures produce gels that are more stable in water. BSA cured at 90 °C remains highly insoluble after one month in water. Initially, $3 \pm 2\%$ (mean \pm std. err.) of protein dissolves and after 30 days, this remains similar at $5 \pm 3\%$ protein loss in water. For 60 °C cured BSA, $35 \pm 5\%$ dissolves in water after 3 days, and this increases to $58 \pm 7\%$ after 30 days ($p = 0.03$). After one month in water, the water-soluble fraction of α -La cured at 90 °C increases from $16 \pm 5\%$ to $27 \pm 3\%$, but not to a statistically different degree ($p = 0.06$). However, even without forming amyloids, α -La does not become completely water-soluble, with the majority solubilizing only after Laemmli dissolution. The amyloid-containing β -Lg also did not dissolve significantly more in water after 30 days ($12 \pm 6\%$ vs. $15 \pm 9\%$; $p = 0.38$).

Table 1. Composition of gels based on solubility in water or Laemmli buffer after soaking in water

for 3 days or 30 days. Error bars represent standard error; n = 3 for each condition.

Protein	Curing Temp (°C)	Time in water (Days)	Water-soluble fraction (%)	Laemmli-soluble fraction (%) ^a	Laemmli-insoluble fraction (%)
β-Lg	70	3	48 ± 8	36 ± 6	16 ± 3
β-Lg	70	30	66 ± 13	29 ± 12	4 ± 2
β-Lg	90	3	12 ± 6	39 ± 10	49 ± 10
β-Lg	90	30	15 ± 9	56 ± 14	29 ± 6
BSA	60	3	35 ± 5	17 ± 6	47 ± 11
BSA	60	30	58 ± 7	22 ± 4	20 ± 9
BSA	90	3	3 ± 2	16 ± 7	81 ± 7
BSA	90	30	5 ± 3	14 ± 8	81 ± 6
α-La	60	3	39 ± 6	37 ± 6	25 ± 10
α-La	60	30	65 ± 12	30 ± 11	5 ± 2
α-La	90	3	16 ± 5	34 ± 3	51 ± 7
α-La	90	30	27 ± 3	58 ± 11	16 ± 8

^aWater insoluble; Laemmli buffer consists of 2% SDS, 10% glycerol, 5% beta-mercaptoethanol, 0.5% bromophenyl

blue

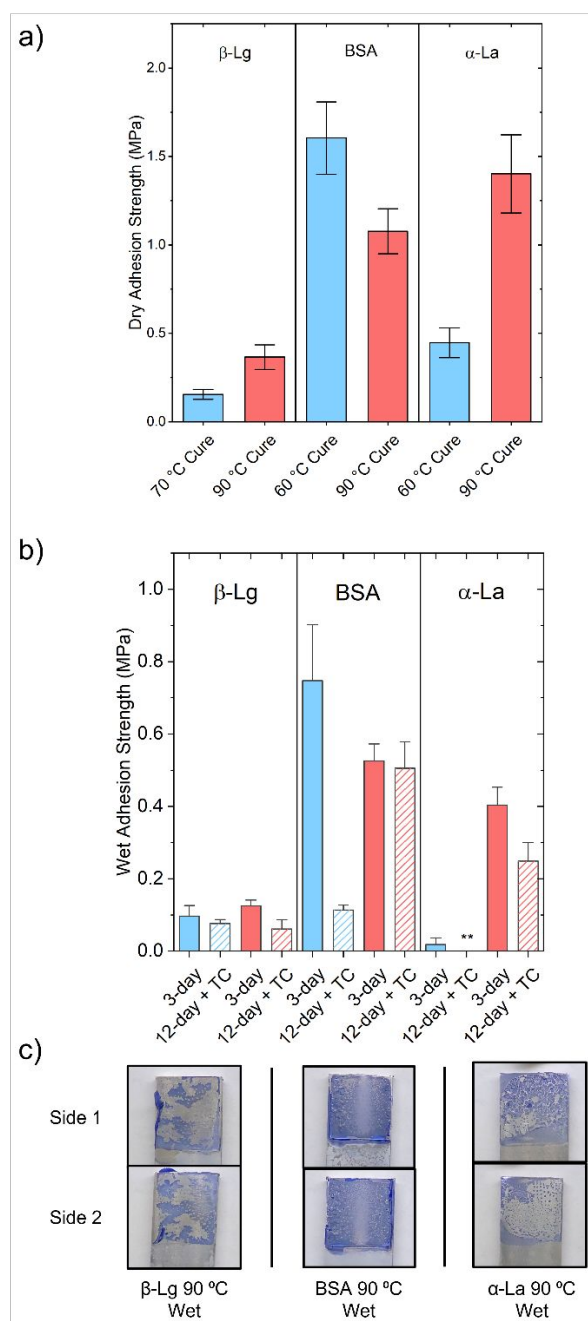


Figure 4. Lap shear results. a) Lap shear adhesion strength after equilibration in desiccator for around three days. b) Lap shear adhesion strength after equilibration in water for around three days (short term) or after 12 days in water followed by thermal cycling (TC). ** α -La cured at 60 °C

was not tested with 12-day and TC because of poor performance in 3-day conditioned samples. c) Pictures of lap shear sample stained to highlight failure mode. Top and bottom pictures reflect the two sides of the lap shear sample.

Using the same curing conditions, we then fabricate adhesives exposed to both dry and wet conditions and test their strength by lap shear (Figure 4, Figure S19). Steam curing is a viable approach to cure proteins into model adhesive structures at the contact. This is in contrast to BSA solutions heated by dry oven at the same temperatures which did not adhere in previous literature.²⁵

The dry and wet adhesion among the proteins followed a similar trend, with BSA at both temperatures performing well, along with α -La cured at high temperature. For BSA at 40% (w/v) cured at 60 °C on polished aluminum, samples attain 0.74 ± 0.16 MPa (*mean \pm standard error*) after soaking in water for three days. When curing the same concentration solution at 90 °C, samples attain 0.53 ± 0.05 MPa in wet conditions. The wet adhesion for β -Lg cured at 90 °C was only 0.12 ± 0.02 MPa, with samples cured at 70 °C obtaining a similar value at 0.10 ± 0.03 MPa. The α -La achieved 0.40 ± 0.05 MPa in wet conditions when cured at 90 °C, but when curing at 60 °C, six of the seven samples submerged in water failed before loading (0.02 ± 0.02 MPa). Samples failed cohesively for BSA under both curing conditions after either wet or dry conditioning (Figure

4c, Figure S20). The samples of β -Lg and α -La in both curing conditions failed adhesively or mixed adhesively/cohesively when wet (Figure 4c, Figure S20).

We further tested the wet adhesion with thermal cycling to simulate long-term conditioning (Figure 4b). BSA samples cured at 90 °C were still able to retain full adhesion strength in heated water (0.51 ± 0.07 MPa). BSA cured at 60 °C showed a dramatic decrease in adhesion strength after thermal cycling (0.11 ± 0.01 MPa), retaining less than 20% of its short-term wet adhesion. The adhesion strength for α -La dropped nearly in half upon long-term soaking and heating (0.25 ± 0.5 MPa, $p = 0.03$). For β -Lg, adhesive performance was generally poor across tested samples (0.08 ± 0.01 for 70 °C curing and 0.06 ± 0.03 MPa for 90 °C curing). Notably, two of the samples for 70 °C and one sample for 90 °C curing performed extraordinarily well for β -Lg after thermal cycling (between 1-1.4 MPa), even exceeding the dry adhesion of β -Lg samples. Heat has been shown to cause changes in β -Lg structure and thereby adhesion,⁵¹ which could be subject for further research. For this study, though, these samples were discarded as outliers.

DISCUSSION

Processing conditions that achieve model amyloid and non-amyloid protein structures allow us to understand the contribution of aggregation state on adhesive performance underwater. Samples cured at high temperatures for β -Lg and BSA can be used to highlight properties of amyloid materials. Conversely, samples cured at low temperatures for β -Lg and BSA can be used to determine adhesive properties that stem from aggregation with minimal contributions from amyloids. Lastly, under our processing, α -La does not form amyloids, but retains β -sheet/extended conformations when cooled to room temperature. In previous research, α -La has been shown to form amyloids at low pH,^{30,52} after proteolysis,⁵³ and heating in reducing conditions,²⁸ but not with temperature alone.²⁸ In our case, even at high concentration, α -La did not convert into amyloids using temperature (Figure 3c). However, α -La can be used as a comparison to β -Lg and BSA, as it is heated to the same temperatures (60 °C and 90 °C) but yields a different structure.

Overall, temperatures where secondary structures transition for protein gels agree with conditions which show measurable changes in solubility. Structural transitions are observed to lead to greater material stability underwater. For β -Lg, protein structure changes in degree of ordering by 90 °C (Figure 3b), in agreement with a significant shift in gel solubility between 70 °C and 80 °C (Figure 2e). BSA gels, on the other hand, more dramatically convert into β -sheets

from RT to 90 °C (Figure 3b), corresponding also to a gradual shift at each temperature towards greater insolubility (Figure 2e). α -La has markedly altered structure at 90 °C compared to 60 °C, which corresponds to large differences in solubility at 60 °C and 90 °C. Gains in underwater gel stability are not unique to amyloid structures (Table 1). For example, β -Lg reaches *ca.* 45% insoluble content at the highest cure temperature (compared to 81% for BSA), like the non-amyloid α -La. Observed changes in solubility with temperature match previous understanding of mechanism for the aggregation of these proteins. At lower curing temperatures (65-80 °C), disulfide bond shuffling is the predominant mechanism of aggregation.⁵⁴ Other types of chemical modifications are minimal.⁵⁵ At higher temperatures (>80 °C), restructuring from non-covalent interactions occurs.⁵⁴ In the case of our high concentration solutions, this non-covalent restructuring includes the formation of insoluble amyloids. Amyloid-enriched materials demonstrated resistance to being dissolved when exposed to water for 30 days, where most all other proteins and aggregate types showed material loss either within days of immersion or after long-term soaking in water. Further degradation by denaturing chemistries reveals that not all amyloids are chemically robust, where β -Lg gels containing amyloids can be more readily

dissolved by Laemmli buffer while amyloids comprised of BSA remain mostly Laemmli-insoluble.

The structure and stability of gels largely translated to their underwater properties as cure-in-place adhesives. In general, the dry and wet bond strengths followed the same general trend (Figure 4), regardless of protein and processing. The adhesives which performed well as dry adhesives also generally performed well as wet adhesives, though all adhesives performed better in dry conditions than in wet conditions. Water interferes with both bulk and interfacial adhesion,⁵⁶ so a decrease in adhesion strength is expected. Though no clear trend arose between amyloids and dry bond strength, protein aggregation achieved in this work led to gains in long-term adhesive underwater performance for BSA. Overall, BSA performed well as an adhesive across all conditions. A direct correlation could be seen for BSA between conversion into beta sheet content at increased curing temperature and gains in underwater performance of the material. This led to significant enhancements in long-term adhesive performance, where full bond strength was retained even after 12 days of soaking and thermal cycling while BSA cured at low temperatures lost 80% bond strength under the same conditions. Conversely, α -La cured at 90 °C provides a counterexample. Like BSA, protein aggregation provides short-term wet adhesion, but after long-

term soaking and thermal cycling, it loses adhesive strength (Figure 4b). The overall solubility of α -La cured at 90 °C did not shift to a statistically significant degree between 3 and 30 days in water, however chemical denaturants were able to dissolve a greater degree from the 30-day samples than from 3-day samples, removing $58 \pm 11\%$ compared to $34 \pm 3\%$ (Table 1). α -La cured at 90 °C became more susceptible to similar chemical denaturant treatment after long periods in water, indicating that the biophysical state of aggregates in α -La alters over time. Though amyloids demonstrated substantially better underwater stability over their non-amyloid counterparts as free gels, we were unable to determine if they provide similar gains to adhesives across proteins. β -Lg remained a poor adhesive throughout all processing conditions and failed at the metal interface before enhancements to bulk adhesion could be measured. Protein composition did not explain the poor performance of β -Lg compared to BSA or α -La, in light of the importance of polar and charged residues previously attributed to the success of barnacle proteins.⁵⁷ β -Lg and α -La share a similar fraction of charged residues (Asp, Glu, Lys, and Arg), while β -Lg and BSA share a similar fraction of polar residues (Ser, Thr, Gln, and Asn). The poor adhesive results from β -Lg show that amyloids must be paired with a protein capable of adhesion, while our model BSA adhesive shows promise in how amyloids can contribute to underwater performance.

The stability of amyloids provides one function that may help organisms like barnacles produce successful glues. While the cement protein chemistry itself may dictate the adhesive strength, success across environments is a necessary factor. Their plaque must combat dry and wet conditions, high salinity, temperature swings, and cyclical wave action. Secreted as part of the molting process in acorn barnacles,⁵⁸ deposited adhesive must last until enough new material is generated. In our case, we used temperature to control the structure of proteins and saw that certain amyloids are capable of wet adhesion. Barnacles use careful control of their sequence to assemble protein materials.⁵⁹ Additionally, these sequences may have been evolved with adhesive performance as a pressure. This requirement of stability might also help explain why both stalked and acorn barnacles use amyloids in their plaque.^{9, 60, 61} Since all barnacles encounter harsh environments, amyloids may persist across barnacle species despite divergence of stalked and acorn barnacles in many other facets of their plaque use.

CONCLUSION

In this work, we have developed simple model protein glues by triggering their phase transformation at the adhesive contact using heat. Using solutions of only protein and water, we are able to probe the effects of protein aggregation state on their ability to survive underwater

conditions and maintain bonds. We find that while amyloids do not dramatically improve adhesive strength of bonded materials, they can greatly enhance long-term stability of the adhesives underwater. Our results shed light on why amyloid structures are prevalent in natural adhesives and what functions amyloid structures could bring to bioinspired adhesives. Separate from particular bioinspired chemistries or added crosslinking chemistries, we show that aggregation state can control the long-term underwater performance of protein-based adhesives. As many commercial proteins can form amyloids, our results pave the way for further study of amyloid-based adhesives and their use in underwater applications.

AUTHOR CONTRIBUTIONS

Michael Wilson: Conceptualization, Methodology, Investigation, Visualization, Writing –

Original Draft. **Maryssa Beasley:** Methodology, Investigation, Formal Analysis. **Kenan Fears:**

Investigation. **Elizabeth Yates:** Methodology, Formal Analysis. **Christopher So:**

Conceptualization, Visualization, Supervision, Writing - Review & Editing. The manuscript was

written through contributions of all authors. All authors have given approval to the final version

of the manuscript.

CONFLICTS OF INTEREST

There are no conflicts to declare.

ACKNOWLEDGMENTS

This work was funded by the Office of Naval Research biomaterials and bionanotechnology program (N0001419WX01085 and N0001422WX00892). This research was performed while M.C.W. and M.A.B. held an NRC Research Associateship award at the Naval Research Laboratory. E.A.Y. was supported through the NRL-United States Naval Academy Cooperative Program for Scientific Interchange (N0017321WX00309 and N0017322WX00257). The authors would like to thank Dr. Daniel E. Barlow and Dr. Cynthia G. Pyles for helpful advice about infrared spectroscopy.

REFERENCES

1. M. R. Chapman, L. S. Robinson, J. S. Pinkner, R. Roth, J. Heuser, M. Hammar, S. Normark and S. J. Hultgren, *Science*, 2002, **295**, 851-855.

2. T. Priemel, G. Palia, F. Förste, F. Jehle, S. Sviben, I. Mantouvalou, P. Zaslansky, L. Bertinetti and M. J. Harrington, *Science*, 2021, **374**, 206-211.
3. M. J. Sever, J. T. Weisser, J. Monahan, S. Srinivasan and J. J. Wilker, *Angew. Chem. Int. Ed.*, 2004, **43**, 448-450.
4. K. Kamino, M. Nakano and S. Kanai, *FEBS J.*, 2012, **279**, 1750-1760.
5. D. K. Burden, D. E. Barlow, C. M. Spillmann, B. Orihuea, D. Rittschof, R. Everett and K. J. Wahl, *Langmuir*, 2012, **28**, 13364-13372.
6. P. Cheung, G. Ruggieri and R. Nigrelli, *Mar. Biol.*, 1977, **43**, 157-163.
7. N. N. Ashton, D. S. Taggart and R. J. Stewart, *Biopolymers*, 2012, **97**, 432-445.
8. A. S. Mostaert, M. J. Higgins, T. Fukuma, F. Rindi and S. P. Jarvis, *J. Biol. Phys.*, 2006, **32**, 393-401.
9. D. E. Barlow, G. H. Dickinson, B. Orihuea, J. L. Kulp III, D. Rittschof and K. J. Wahl, *Langmuir*, 2010, **26**, 6549-6556.
10. E. B. Sawyer, D. Claessen, M. Haas, B. Hurgobin and S. L. Gras, *PLoS One*, 2011, **6**, e18839.
11. D. S. Capstick, A. Jomaa, C. Hanke, J. Ortega and M. A. Elliot, *Proc. Natl. Acad. Sci. U.S.A.*, 2011, **108**, 9821-9826.
12. H. A. Wösten and M. L. de Vocht, *Biochimica et Biophysica Acta (BBA)-Reviews on Biomembranes*, 2000, **1469**, 79-86.
13. M. A. Lambrecht, K. J. Jansens, I. Rombouts, K. Brijs, F. Rousseau, J. Schymkowitz and J. A. Delcour, *Compr. Rev. Food Sci. Food Saf.*, 2019, **18**, 1277-1291.
14. K. J. Jansens, M. A. Lambrecht, I. Rombouts, M. Monge Morera, K. Brijs, F. Rousseau, J. Schymkowitz and J. A. Delcour, *Compr. Rev. Food Sci. Food Saf.*, 2019, **18**, 1256-1276.
15. T. P. Knowles and M. J. Buehler, *Nat. Nanotechnol.*, 2011, **6**, 469-479.
16. T. Fukuma, A. S. Mostaert and S. P. Jarvis, *Tribol. Lett.*, 2006, **22**, 233-237.
17. P. T. Lansbury Jr, *Biochemistry*, 1992, **31**, 6865-6870.
18. Y. Cao and R. Mezzenga, *Adv. Colloid Interface Sci.*, 2019, **269**, 334-356.
19. H. Yin, E. Zhang, Z. Zhu, L. Han, P. Zheng, H. Zeng and N. Chen, *ACS Appl. Polym. Mater.*, 2021, **3**, 1032-1041.
20. C.-Y. Lin and J. C. Liu, *ACS Appl. Bio Mater.*, 2020, **3**, 3894-3905.
21. S. Pradyawong, G. Qi, N. Li, X. S. Sun and D. Wang, *Int. J. Adhes. Adhes.*, 2017, **75**, 66-73.
22. G. Schmidt, B. R. Hamaker and J. J. Wilker, *Adv. Sustain. Syst.*, 2018, **2**, 1700159.
23. Z. Gao, W. Wang, Z. Zhao and M. Guo, *J. Appl. Polym. Sci.*, 2011, **120**, 220-225.

24. G. Wang, T. Zhang, S. Ahmad, J. Cheng and M. Guo, *Int. J. Adhes. Adhes.*, 2013, **41**, 198-205.
25. J. K. Román and J. J. Wilker, *J. Am. Chem. Soc.*, 2018, **141**, 1359-1365.
26. C. R. Frihart and L. F. Lorenz, Protein adhesives. In *Handbook of adhesive technology*. CRC Press: 2017, 145-175.
27. X. Yu, S. Afreen, Q. Kong and J. Wang, *Langmuir*, 2020, **36**, 11975-11984.
28. Y. Cao, J. Adamcik, M. Diener, J. R. Kumita and R. Mezzenga, *J. Am. Chem. Soc.*, 2021, **143**, 11473-11481.
29. L. N. Arnaudov, R. de Vries, H. Ippel and C. P. van Mierlo, *Biomacromolecules*, 2003, **4**, 1614-1622.
30. J. Goers, S. E. Permyakov, E. A. Permyakov, V. N. Uversky and A. L. Fink, *Biochemistry*, 2002, **41**, 12546-12551.
31. V. Vetri, M. D'Amico, V. Foderà, M. Leone, A. Ponzoni, G. Sberveglieri and V. Militello, *Archives of biochemistry and biophysics*, 2011, **508**, 13-24.
32. H. LeVine III, *Methods Enzymol.*, 1999, **309**, 274-284.
33. A. Kamada, M. Rodriguez-Garcia, F. S. Ruggeri, Y. Shen, A. Levin and T. P. Knowles, *Nat. Commun.*, 2021, **12**, 1-10.
34. D. M. Byler and H. Susi, *Biopolymers: Original Research on Biomolecules*, 1986, **25**, 469-487.
35. H. Yang, S. Yang, J. Kong, A. Dong and S. Yu, *Nature protocols*, 2015, **10**, 382-396.
36. Y. Yu, P. Xu, J. Xing, L. Li and J. Chang, *Polym. Eng. Sci.*, 2018, **58**, 1810-1816.
37. N. Okuda and M. Sato, *J. Wood Sci.*, 2007, **53**, 139-142.
38. J. D. White and J. J. Wilker, *Macromolecules*, 2011, **44**, 5085-5088.
39. L. H. Greene, J. A. Grobler, V. A. Malinovskii, J. Tian, K. R. Acharya and K. Brew, *Protein Eng.*, 1999, **12**, 581-587.
40. S. Prabakaran and S. Damodaran, *J. Agric. Food Chem.*, 1997, **45**, 4303-4308.
41. B. Jiang, A. Jain, Y. Lu and S. W. Hoag, *Mol. Pharm.*, 2019, **16**, 3687-3693.
42. J. Gezimati, L. K. Creamer and H. Singh, *J. Agric. Food Chem.*, 1997, **45**, 1130-1136.
43. J. I. Boye, I. Alli and A. A. Ismail, *J. Agric. Food Chem.*, 1997, **45**, 1116-1125.
44. R. Kodali and R. Wetzel, *Curr. Opin. Struct. Biol.*, 2007, **17**, 48-57.
45. G. P. Gellermann, H. Byrnes, A. Striebinger, K. Ullrich, R. Mueller, H. Hillen and S. Barghorn, *Neurobiol. Dis.*, 2008, **30**, 212-220.

46. T. J. Huang, D.-S. Yang, N. P. Plaskos, S. Go, C. M. Yip, P. E. Fraser and A. Chakrabartty, *Journal of molecular biology*, 2000, **297**, 73-87.
47. A. Roher, D. Wolfe, M. Palutke and D. KuKuruga, *Proc. Natl. Acad. Sci. U.S.A.*, 1986, **83**, 2662-2666.
48. C. L. Masters, G. Simms, N. A. Weinman, G. Multhaup, B. L. McDonald and K. Beyreuther, *Proc. Natl. Acad. Sci. U.S.A.*, 1985, **82**, 4245-4249.
49. M. Lindgren and P. Hammarström, *FEBS J.*, 2010, **277**, 1380-1388.
50. H. Fabian, G. I. Szendrei, M. Jackson, W. C. Halliday, L. Otvos and H. H. Mantsch, *Appl. Spectrosc.*, 1993, **47**, 1513-1518.
51. S. W. Lee, H. Choi, G. Lee, Y. Choi, H. Lee, G. Kim, H. Lee, W. Lee, J. Park and D. S. Yoon, *ACS Macro Letters*, 2021, **10**, 1549-1554.
52. R. Mishra, *Protein Sci.*, 2021, **30**, 1919-1934.
53. J. Otte, R. Ipsen, R. Bauer, M. J. Bjerrum and R. Waninge, *International dairy journal*, 2005, **15**, 219-229.
54. J. De Wit, *Trends Food Sci. Technol.*, 2009, **20**, 27-34.
55. C. Li, S. B. Nielsen, K. Engholm-Keller and M. N. Lund, *J. Agric. Food Chem.*, 2022, **70**, 4391-4406.
56. J. H. Waite, *Int. J. Adhes. Adhes.*, 1987, **7**, 9-14.
57. Y. Urushida, M. Nakano, S. Matsuda, N. Inoue, S. Kanai, N. Kitamura, T. Nishino and K. Kamino, *The FEBS Journal*, 2007, **274**, 4336-4346.
58. K. P. Fears, B. Orihuela, D. Rittschof and K. J. Wahl, *Adv. Sci.*, 2018, **5**, 1700762.
59. C. R. So, E. A. Yates, L. A. Estrella, K. P. Fears, A. M. Schenck, C. M. Yip and K. J. Wahl, *ACS nano*, 2019, **13**, 5172-5183.
60. J.-L. Jonker, L. Morrison, E. P. Lynch, I. Grunwald, J. von Byern and A. M. Power, *Interface Focus*, 2015, **5**, 20140062.
61. M. A. Tilbury, S. McCarthy, M. Domagalska, T. Ederth, A. M. Power and J. G. Wall, *Philos. Trans. R. Soc. Lond., B, Biol. Sci.*, 2019, **374**, 20190205.

